3D wavefield tomography: synthetic and field data examples

Mike Warner, Ivan Stekl and Adrian Umpleby, Earth Science and Engineering, Imperial College London*

Summary

Full wavefield tomography has become well established in two dimensions, but its extension into 3D for realistically sized problems is computationally daunting. In this paper, we present one of the first studies to apply 3D wavefield tomography to field data, and demonstrate that the method can solve useful exploration problems that that are not tractable by other methods.

Introduction

Following the pioneering work of Gerhard Pratt and co-workers who developed the first frequency-domain direct solvers for the acoustic wave equation for cross-hole data, wavefield seismic tomography is now well developed in two dimensions. Their work has been extended and developed, and time-domain, visco-acoustic, elastic and anisotropic schemes have appeared, and have been applied to a wide variety of source-receiver geometries. Recently, these 2D methods have begun to be extended into three-dimensions where their full potential can be realized.

In 2D, two principal methods have been used to perform wavefield tomography – direct factorization of the matrix equations obtained by applying finite differences to the wave equation in the frequency domain, and explicit time-stepping of the finite difference equations in the time-domain. The two approaches both have their own advantages and problems, and both have recently been extended into three dimensions and applied to synthetic datasets. Both methods are computationally daunting in three dimensions.

We have chosen a third route; we solve the frequency-domain finite-difference matrix equations in 3D using an iterative rather than a direct solver. In this approach, we first solve an approximate matrix equation (the preconditioning matrix) for a particular source. This approximate solution is then substituted into the true matrix equations to derive a residual error. This error is then treated as a new source for which we can obtain an approximate solution, and the method is iterated.

The advantage of our approach over that of a direct solution by, for example LU decomposition and nested dissection, is that the memory required in 3D is typically reduced by several orders of magnitude. Thus the iterative method can be implemented on a single workstation rather than distributed across a large cluster. The advantage over the time-domain method is that, provided that only a few frequencies are required for tomography, the compute time taken for one source is typically much less in the frequency domain than in the time domain.

There are also some disadvantages to our approach. Using a direct solution in the frequency domain has the advantage over our method that multiple sources may be obtained relatively cheaply by back substitution once the initial factorization has been completed. However in 3D this disadvantage is largely disappears since the computational effort required to obtain an iterative solution for a single source is typically no larger than that required to obtain the solution by back substitution, but in the latter, the memory required is much greater. The time-domain has the advantage that there is a near-one-to-one relationship between a particular part of the seismic data and a particular part of the earth model. This means that simple processing of the seismic data, especially muting, weighting and filtering, can be readily integrated within a time-domain tomographic scheme, and readily quality controlled, in ways that are difficult or impossible in the sparse frequency-domain.

Method

The key to obtaining an efficient and effective iterative solver is the appropriate choice of both the preconditioning matrix and the method used to calculate the iterative update. We have tried many variants of preconditioner and found that most methods that work well in other areas of computational physics perform badly or fail entirely for the wave equation. Currently we use three levels of preconditioner:

- At the lowest level, we use a simple one-way propagator that propagates energy a distance of about 20 cells across the model. We sweep this in six orthogonal directions, up-down, back-front and left-right. This approximate solution is then iterated with the full two-way wave equation so that we obtain the full solution to the two-way equation.

- At a higher level, we use a multi-grid approach. Here, we first solve the wave equation on a coarse grid. This coarse solution serves as a preconditioner for a more accurate solution on a finer grid. For the lowest frequencies, the coarsening of the mesh may involve several stages, halving the grid spacing at each step. We use a 27- point cubic finite-difference stencil that is formally second-order in space but which performs with

a numerical accuracy equivalent to a conventional fourth-order stencil at a grid spacing of about 5 grid points per seismic wavelength.

- At the highest level, we divide the model into a small number of over lapping sub-domains. We solve first for the sub-domains separately, then use these as preconditioners to obtain the solution over the entire domain.

The iterative updates use a restarted flexible generalized minimum residual (fGMRES) method, but we find that it is necessary only to store and use one generation of previous results to obtain optimal convergence which also minimize memory usage.

We have implemented this multi-preconditioned iterative forward solver within a parallel tomographic solver that is also iterative. Within the tomography there are two levels of parallelization:

- A single composite source is solved on a single multi-core/multi-CPU node. POSIX threads are used to balance the computation across all the cores present on the node. The node need be concerned only with that part of the physical model which its source illuminates and which produces seismic returns at its receivers. Typically this region is smaller than that of the global model.

- Additional sources are computed in parallel on additional nodes, and a master node combines the individual results to provide a global update to the model, and control and balance the computation across the cluster.

In an ideal case, the number of nodes will equal the number of sources plus the master node, and individual nodes will have the maximum number of economically available cores – currently eight as quad-core dual-CPUs. Where there are more sources than available nodes, multiple sources may be solved on a single node at a maximum of one source per core provided that there is sufficient memory. Where there is neither sufficient memory or sufficient cores, then multiple sources are solved sequentially on the same nodes.

An important aspect of our approach is that we combine the data from individual point sources to form a smaller number of composite sources, and perform the tomography on these composite sources. Provided that the number of point sources mixed in this way is not too large, we find that there is no change in the quality of the velocity image that we obtain.

The maximum number of sources that can be mixed, and their optimum geometry depends upon the acquisition geometry and the details of the velocity model; this is still an area of active research. The optimum mix of point sources ranges from all of them combined to form a single composite source which is appropriate when the geometry of the tomographic coverage is near-complete, to around ten to twenty sources mixed together which is appropriate for conventional surface-streamer 3D swath shooting.

Synthetic Results

Figures 1 and 2 show horizontal and vertical cuts through a 3D model of two shallow channels that act as velocity anomalies. The true model is shown as the top panel in each figure. The strike of the two channels is different, and one channel forms a high-velocity and the other a low-velocity anomaly. The channels are only about three seismic wavelengths in width, and are below the typical spatial resolution of travel-time tomographic and migration velocity analysis techniques.

The lower panels in figures 1 and 2 show the results of applying 3D wavefield tomography using composite sources. Only seven composite sources were used in total – far fewer than might be used for a field dataset. The composite sources were each composed of about 300 point sources arranged in rectangular arrays across the strike of the channels. The receivers were a 3D OBC array.

The tomography was performed using 11 separate frequencies with only five iterations per frequency. In synthetic models, using very large numbers of iterations results in almost perfect model recovery. However when applying the same methods to field data, using many more than about five iterations per frequency produces no improvement of the model. This is partly because of noise in the data, but it is more importantly because particular computational models do not match perfectly the propagation of seismic energy in the real earth, ignoring as they do elastic effects, anisotropy, attenuation, free-surface ghosts and multiples, source variability and similar hard-to-model effects. Consequently, the results shown in figure 1 and 2 are realistically representative of the likely performance on real field data.

The starting velocity model used for the tomographic reconstruction was a 1D model. The velocity perturbation within the channel is up to 15% of the background starting model.

Despite the small number of composite sources, both channels are well recovered by the tomography. They are not well recovered by more conventional techniques, nor by 2D wavefield tomography.

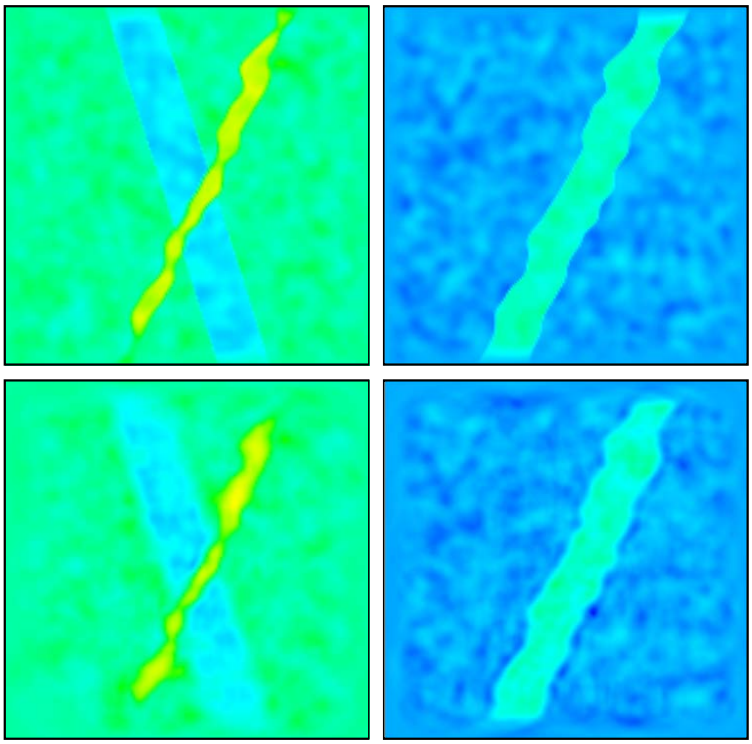

Figure 1 Horizontal slices through a synthetic velocity model of two intersecting channels. The upper panels show the true velocity model, the lower panels show the models recovered by wavefield tomography. The velocity anomaly in the upper channel is recovered in the left panel even when it is less than one seismic wavelength in lateral extent.

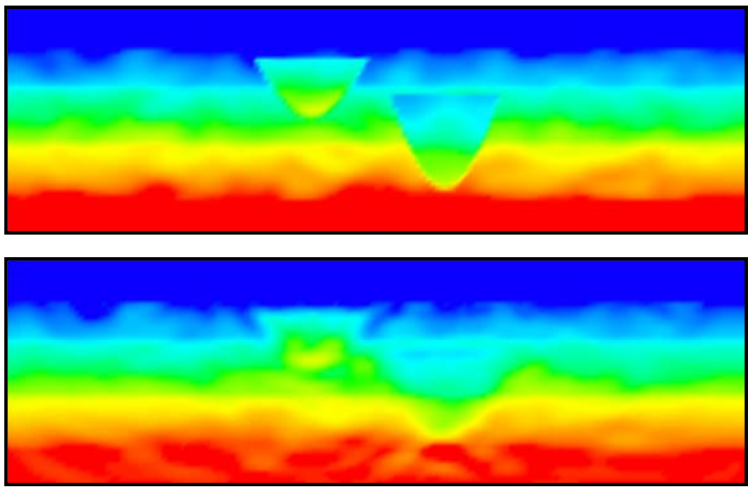

Figure 2 Vertical slices through the model from figure 1. The upper panel shows the true velocity model, the lower panel shows the model recovered by wavefield tomography.

Field Data Results

We have applied our tomographic scheme to the field data shown in figure 3. These 3D data are from an 8-streamer dual-source flip-flop conventional swath survey in the North Sea with a cable length of 5000 m and cable separation of 100 m. The data contain shallow 3D high-velocity channels at a depth of around 1500 m.

These channels produce pull-up on what appear to be otherwise smooth sub-horizontal reflectors beneath, and on the deeper reservoir. The channels also produce a characteristic w-pattern in high resolution stacking velocity analysis also shown in figure 3. The combined effect of the pull up and distorted velocity analysis compromises imaging of the reservoir, and has prevented accurate depth migration leading to increased uncertainty in reserve estimation.

The velocity structure within the channels appears laterally complicated, and it has not been satisfactorily resolved using reflection tomography or migration velocity analysis. Full-wavefield tomography has been applied to this dataset, and the results are shown in figure 4.

The top panel in figure 4 shows the results of depth converting the data using results from conventional velocity analysis. There is clear but complicated velocity distortion of the event at the base of this section underneath the channel. The lower panel shows the same data depth-converted using the high-resolution velocity model obtained from wavefield tomography. Using this velocity model, the reflector at the base of the section appears much simpler in depth, and the velocity distortion produced by the channel appears to have disappeared.

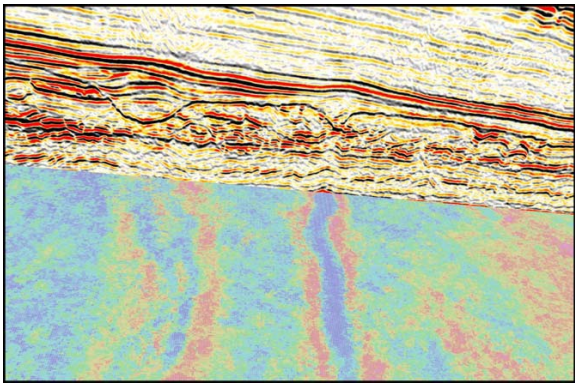

Figure 3 A 2D slice through a 3D seismic survey showing shallow high-velocity channels. The velocity structure in the channels produces a characteristic spurious w-structure in the high-resolution stacking velocity analysis below.

Within the channel itself, the reflector geometry is also subtly but significantly different. In the top pannel, the channel appears to show the effects of clear and systematic differential compaction which is not readily apparent in panel beneath, and the structure of the double sub-channel within the main channel is both clearer and more geologically plausible.

Although conventional methods are unable to image this velocity structure, we conclude that the waveform tomography is producing a high-resolution velocity model that more faithfully represents the sub-surface.

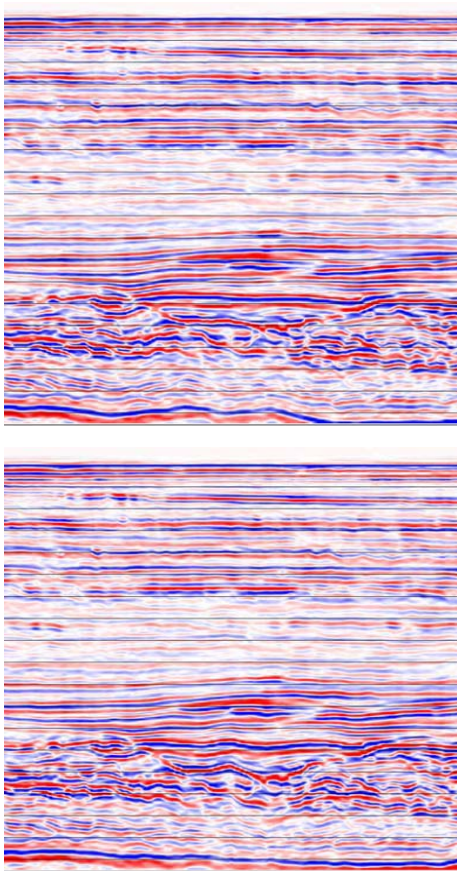

Figure 4 A close up of the pre-stack, time-migrated image of one of the channels and underlying sub-horizontal reflector. The top panel has been depth converted using the original conventionally obtained velocity model. The bottom panel has been depth converted using the high-resolution velocity model obtained from wavefield tomography.

EDITED REFERENCES

Note: This reference list is a copy-edited version of the reference list submitted by the author. Reference lists for the 2008 SEG Technical Program Expanded Abstracts have been copy edited so that references provided with the online metadata for each paper will achieve a high degree of linking to cited sources that appear on the Web.

REFERENCES

none